Supporting Information

Multivariate MOF-303/MIL-160 balancing the trade-off between capacity and selectivity in CO_2/CH_4 separation

Mingming Xu,[a,b] Xiaokang Wang,*[a] Jingjing Chen,[a] Meng Sun,[a] Xueyan Zhang,[a] Weidong Fan,*[a] Tingyi Wang*[b] and Daofeng Sun*[a]

[a]Shandong Key Laboratory of Intelligent Energy Materials, State Key Laboratory of Heavy Oil Processing, School of Materials Science and Engineering, China University of Petroleum (East China), Qingdao, Shandong 266580, China.
[b]Technology Inspection Center, Shengli Oilfield Company, SINOPEC, Dongying, Shandong, 257000, China.

*Corresponding author E-mail: dfsun@upc.edu.cn; wdfan@upc.edu.cn; xiaokangwang0625@163.com; wangtingyi180.slyt@sinopec.com

Table of Contents

Experimental Procedures

Materials and instruments

All reagents were commercially available and used without further purification.

^{1}H Nuclear Magnetic Resonance (NMR) spectra were obtained on a Bruker 600 MHz NEO nuclear magnetic resonance spectrometer. Powder X-ray diffraction (PXRD) was carried out on a Bruker D8-Focus Bragg-Brentano X-ray powder diffractometer equipped with a Cu sealed tube at 40 kV and 15 mA. Scanning electron microscopy (SEM) images were taken with Hitachi Regulus8100 scanning electron microscope. Gas sorption measurements were conducted on a Micrometritics ASAP 2020 surface area analyzer. Breakthrough experiments were carried out on BSD-MAB multi-component adsorption breakthrough curve analyzer monitored by Hiden HPR-20EGA mass spectrometer.

Synthesis of Al-MOFs

Synthesis of MIL-160. A mixture of 2,5-furandicarboxylic acid (FDA) (130 mg, 0.83 mmol), $AlCl_3 \cdot 6H_2O$ (200 mg, 0.83 mmol) and sodium formate (120 mg, 1.76 mmol) in 15 mL deionized H_2O was placed into a glass vial (20 mL) and heated at 100°C for 24 h. The vial was then cooled to room temperature at a rate of 5 °C/h. The obtained white powders were filtered, washed with H_2O and dried in air.

Synthesis of MOF-303. A mixture of 3,5-pyrazoledicarboxylic acid (PDA) (130 mg, 0.83 mmol), $AlCl_3 \cdot 6H_2O$ (200 mg, 0.83 mmol) and sodium formate (120 mg, 1.76 mmol) in 15 mL deionized H_2O was placed into a glass vial (20 mL) and heated at 100°C for 24 h. The vial was then cooled to room temperature at a rate of 5 °C/h. The obtained white powders were filtered, washed with H_2O and dried in air.

Synthesis of MOF-303/MIL-160. A mixture of FDA (65 mg, 0.415 mmol), PDA (65 mg, 0.415 mmol), $AlCl_3 \cdot 6H_2O$ (200 mg, 0.83 mmol) and sodium formate (120 mg, 1.76 mmol) in 15 mL deionized H_2O was placed into a glass vial (20 mL) and heated at 100°C for 24 h. The vial was then cooled to room temperature at a rate of 5 °C/h. The obtained white powders were filtered, washed with H_2O and dried in air.

Gas sorption measurements

The activated samples were prepared by immersing the as-synthesized MOFs in deionized water for solvent exchange followed by activation at 423 K under vacuum for 12 h. Gas adsorption experiments containing N_2 at 77 K, as well as CO_2 and CH_4 at 273 and 298 K, were performed by using ASAP-2020 surface area analyzer. The Brunauer-Emmett-Teller (BET) specific surface area and the pore size distribution were calculated based on the N_2 adsorption isotherm at 77 K. Liquid nitrogen bath was used to stabilize the temperature at 77 K, respectively, whereas other test temperatures were maintained via a circulating water bath. The Brunauer-Emmett-Teller (BET) surface area was calculated using multi-point BET equation with the P/P_0 range of 0.005-0.035. Pore volume was calculated with the maximal adsorption capacity.

Breakthrough experiments

Breakthrough experiments were carried out on BSD-MAB multi-component adsorption breakthrough curve analyzer. The activated samples of multivariate MOF-303/MIL-160 (0.4419 g) were packed in a quartz tube (4 mm inner diameter × 210 mm length) and further flushed with He (≥ 99.99%) at 393 K for 10 h with a flow rate of 15 mL/min. During the experiments at 298 K, the equimolar CO_2/CH_4 (≥ 99.99%) mixture was used at a flow rate of 2 mL/min, and the outlet gas was monitored by Hiden HPR-20EGA mass spectrometer. Between each breakthrough cycle, the samples were regenerated at 393 K for 2 h with He at a flow rate of 15 mL/min. The humidity control part was integrated in BSD-MAB analyzer. The gases were humidified by a widely used bubble humidification method, by which the gases could pass through a tailor-made temperature-regulated humidification bottle with water inside. The humid environments were created by introducing test gases into water until the water signal in mass spectrometer was steady before breakthrough experiment.

Computational methods

Isosteric heat of adsorption

A Virial equation comprising the temperature-independent parameters a_i and b_j was employed to calculate the enthalpies of adsorption for CO_2 and CH_4, which were measured at 273 and 298 K.

$$\ln P = \ln N + \frac{1}{T}\sum_{i}^{m} a_i N_i + \sum_{j}^{n} b_j N_j$$

$$Q_{st} = -R\sum_{i=0}^{m} a_i N_i$$

Here, P is the pressure expressed in mmHg, N is the amount absorbed in mmol/g, T is the temperature in K, a_i and b_j are virial coefficients, and m, n represent the number of coefficients required to adequately describe the isotherms (herein, m =5 and n = 2). Q_{st} is the coverage-dependent isosteric heat of adsorption and R is the universal gas constant.

Selectivity based on ideal adsorbed solution theory

Before estimating the selectivity for binary gas mixture, the single-component gas adsorption isotherms were first fitted to dual-site Langmuir-Freundlich (DSLF) model:

$$q = q_{A,sat}\frac{b_A p^{n_1}}{1 + b_A p^{n_1}} + q_{B,sat}\frac{b_B p^{n_2}}{1 + b_B p^{n_2}}$$

where q is the amount of adsorbed gas (mmol/g), p is the bulk gas phase pressure (kPa), q_{sat} is the saturation amount (mmol/g), b is the Langmuir-Freundlich parameter (kPa^{-1}), and n is the Langmuir-Freundlich exponent (dimensionless) for two adsorption sites A and B indicating the presence of weak and strong adsorption sites. b_A and b_B are both temperature-dependent.

$$b_A = b_{A0}\exp\left(\frac{E_A}{RT}\right);\ b_B = b_{B0}\exp\left(\frac{E_B}{RT}\right)$$

The adsorption selectivity S_{ads} was calculated by ideal adsorbed solution theory:

$$S_{ads} = \frac{q_1/q_2}{p_1/p_2}$$

where q_1 and q_2 are the molar loadings in the adsorbed phase in equilibrium with the bulk gas phase, p_1 and p_2 are partial pressure.

Grand canonical Monte Carlo simulations

Grand canonical Monte Carlo (GCMC) simulations were carried out using the Sorption module of Materials Studio package. The Locate and Metropolis methods were used to predict the possible binding sites of CO_2 and CH_4 onto the framework. During the simulation, the CO_2 and CH_4 molecules including the frameworks were considered as rigid bodies. The optimal adsorption sites were simulated under 298 K and 100 kPa by the fixed loading task and Metropolis method. The atomic partial charges of the host MOF skeleton and all gas molecules were obtained from QEq method. The equilibration steps and the production steps were set to 5.0×10^6 and 1.0×10^7, respectively. The gas-skeleton interaction and the gas-gas interaction were characterized by the standard universal force field (UFF). The cut-off radius used for the Lennard-Jones interactions is 15.5 Å and the long-range electrostatic interactions were considered by the Ewald summation method.

Density functional theory calculations

Density functional theory (DFT) calculations were performed using Dmol3 module embedded in the Materials Studio software. Since it is a vast task to do the DFT calculations using a whole MOF unit cell, we used fragmented cluster models cleaved from unit cells representing the actual situations as high as possible, and the cleaved bonds at cluster boundaries were saturated by protons. The generalized gradient approximation (GGA) with the Perdewe Burkee Ernzerh of (PBE) exchange-correlation functional was employed for the spin-unrestricted DFT calculations. The electronic wave functions were expanded by the double numerical plus polarization (DNP) basis set. The van der Waals correction was considered by Grimme to precisely describe the adsorption of gas molecules on the MOF framework. The convergence criterion was 1×10^5 Ha for energies, 2×10^3 Ha/ Å for forces, and 5×10^3 Å for atomic displacements. The global cutoff radius was set as 6.0 Å. In all the DFT calculations, all the atoms were allowed to fully relax. The adsorption energy (ΔE_{ads}) is expressed

by the equation:

$$\Delta E_{ads} = E_{ads+fram} - E_{fram} - E_{ads}$$

where $E_{ads+fram}$, E_{fram}, and E_{ads} are the total energy of the adsorbate-framework adsorption system, adsorbent framework, and adsorbate molecule, respectively.

Equilibrium adsorption capacity and separation factor

The gas adsorption capacity can be calculated from the breakthrough curves by the equation:

$$q = \frac{F_i t_0 - \int_0^{t_0} F_e dt}{m V_m}$$

where q is the equilibrium adsorption capacity (mmol/g), F_i is the influent flow rate of the specific gas (mL/min), t_0 is the adsorption time (min), F_e is the effluent flow rate of the specific gas (mL/min), m is the mass of the adsorbents (g), and V_m is the molar volume of gas (L/mol).

The separation factor of the breakthrough experiment is determined as:

$$\alpha = \frac{q_1/q_2}{y_1/y_2}$$

where α is the separation factor, q is the equilibrium adsorption capacity, y is the molar fraction of gas.

Figures S1-S25

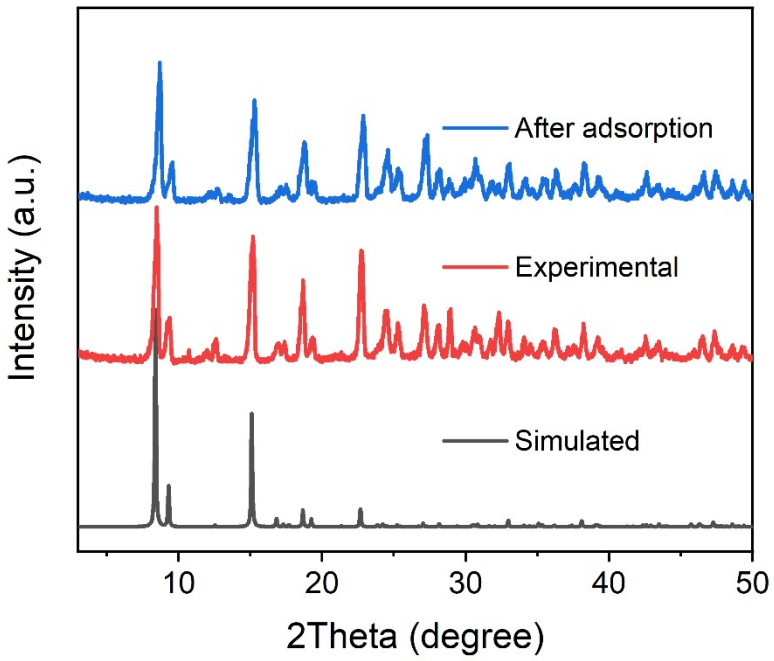

Fig. S1 PXRD patterns of MIL-160.

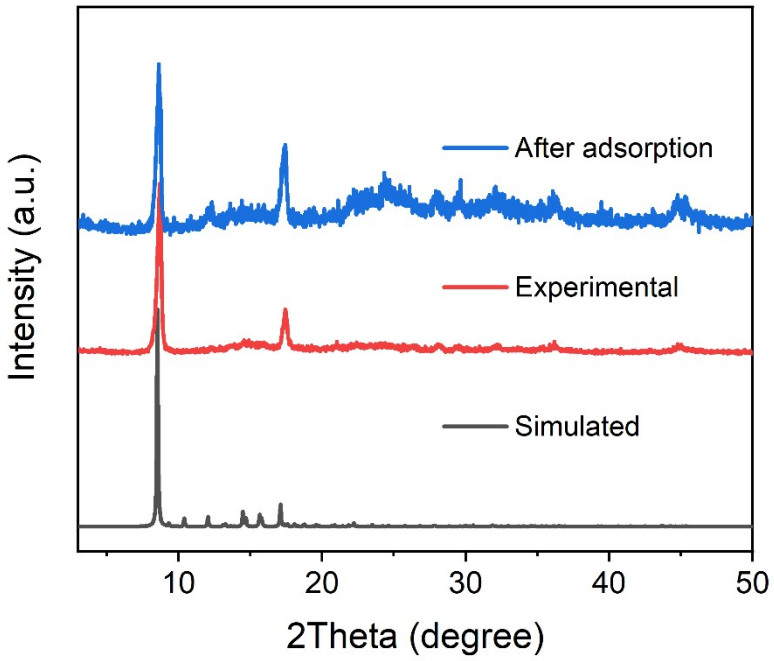

Fig. S2 PXRD patterns of MOF-303.

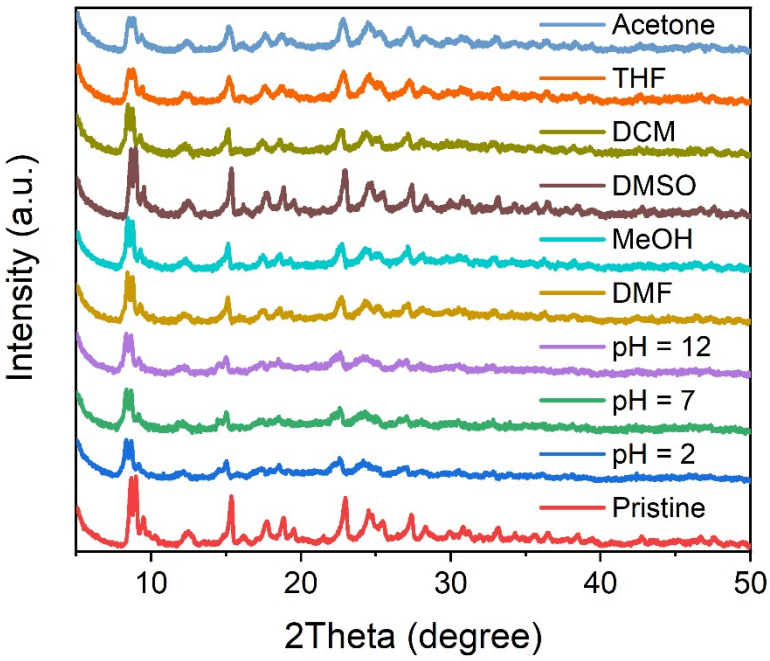

Fig. S3 PXRD patterns of MOF-303/MIL-160 after treatment in different solutions for 24 h.

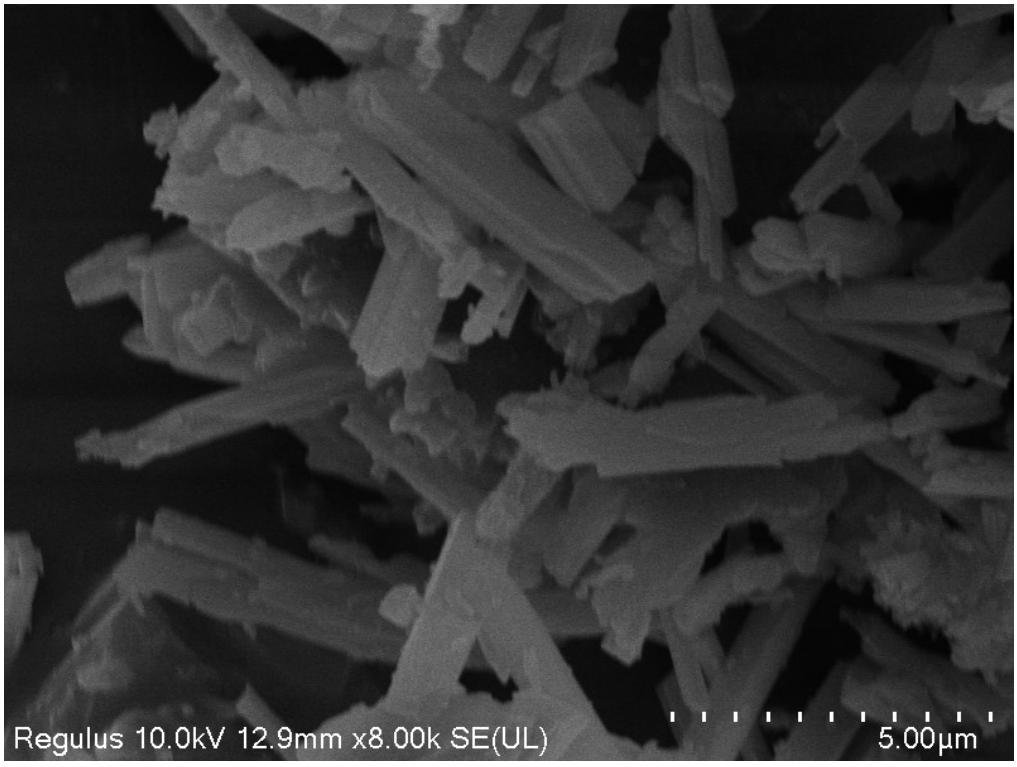

Fig. S4 SEM image of MOF-303/MIL-160.

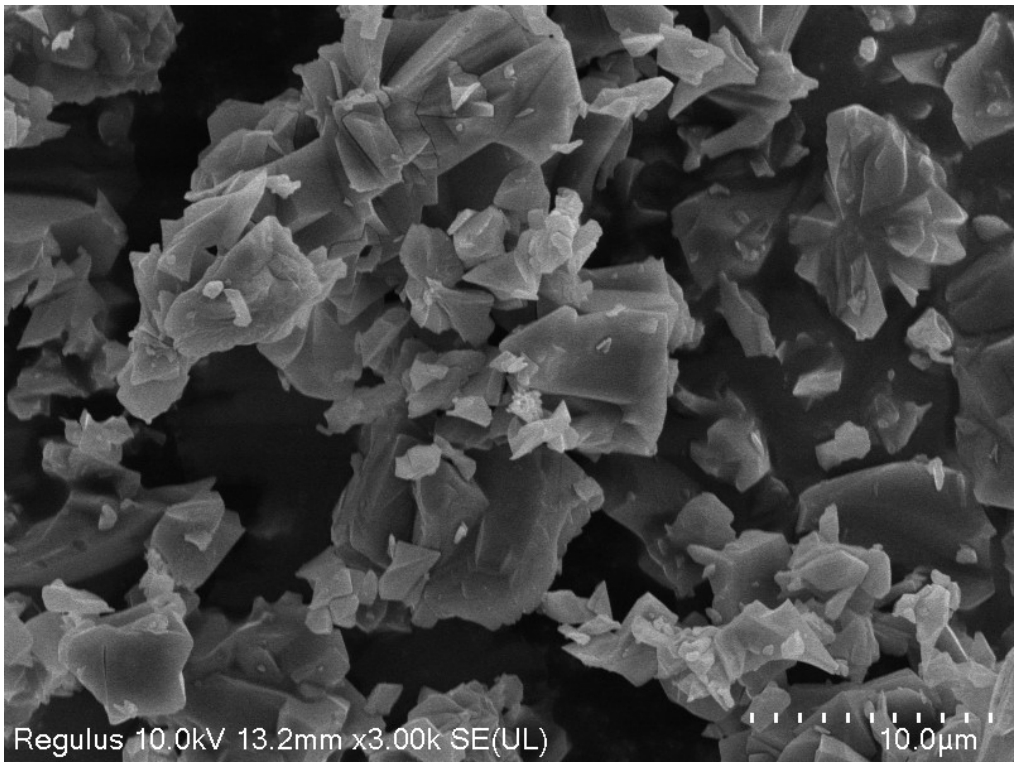

Fig. S5 SEM image of MIL-160.

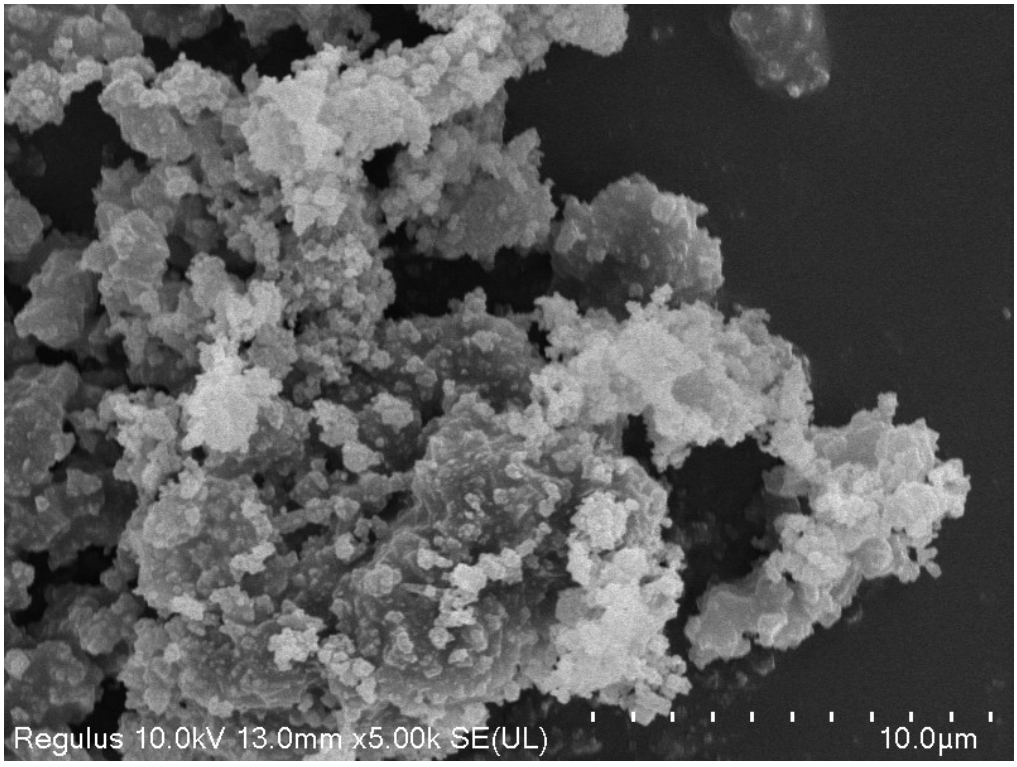

Fig. S6 SEM image of MOF-303.

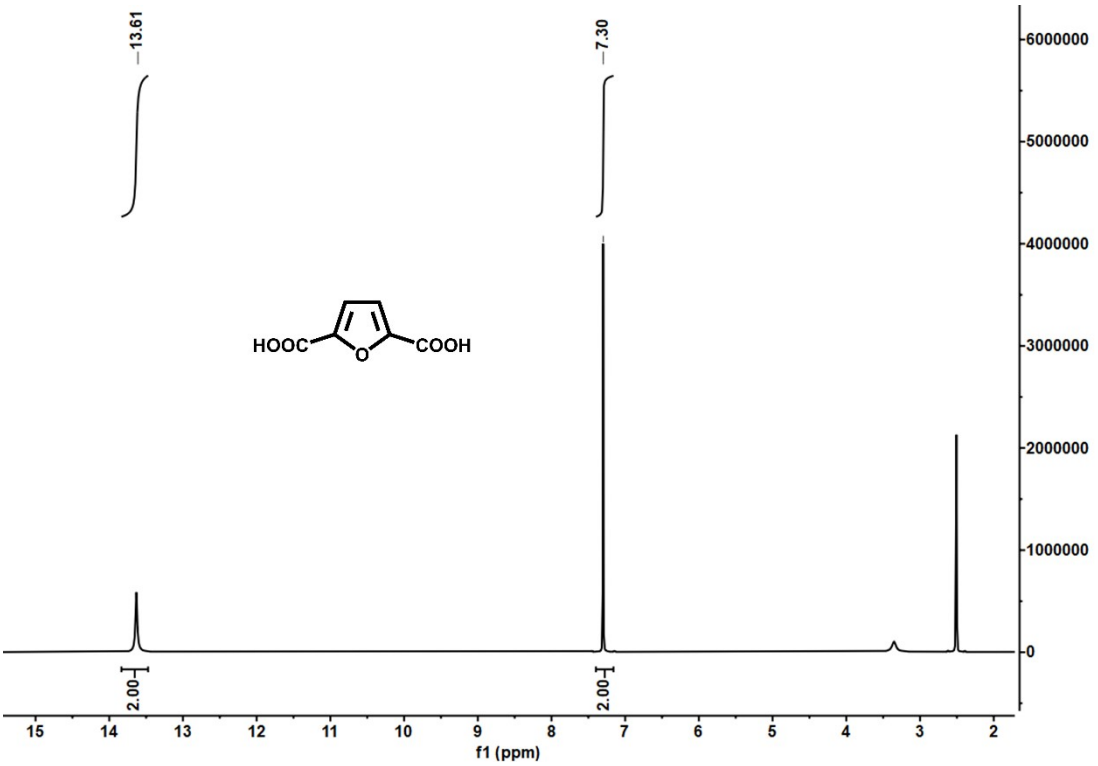

Fig. S7 ^{1}H NMR spectrum of 2,5-furandicarboxylic acid.

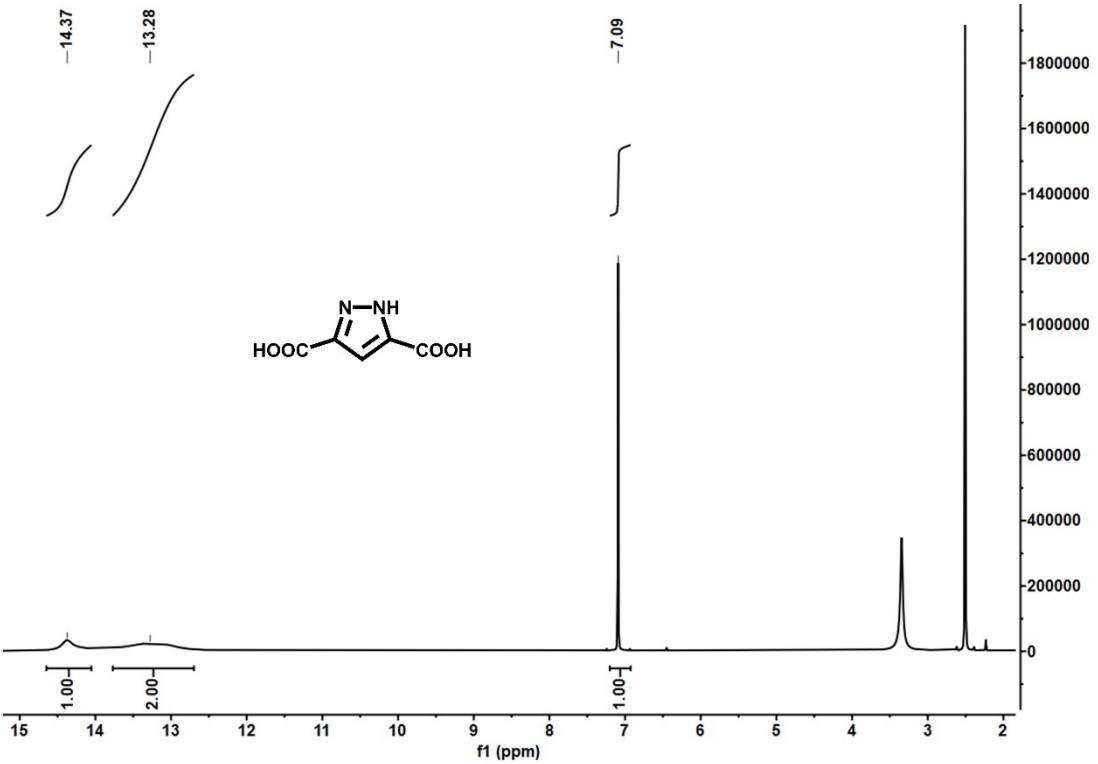

Fig. S8 ^{1}H NMR spectrum of 3,5-pyrazoledicarboxylic acid.

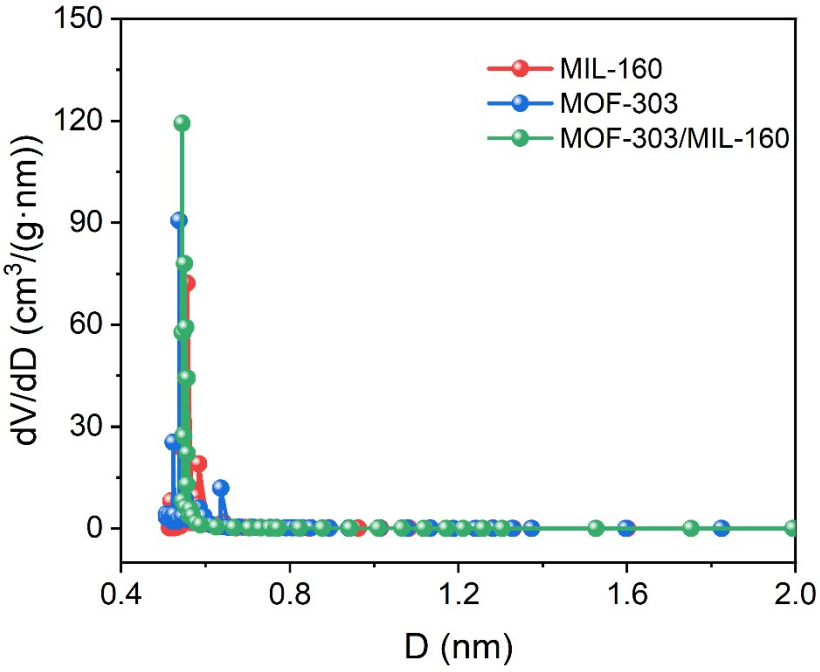

Fig. S9 Pore size distribution of MIL-160, MOF-303, and MOF-303/MIL-160.

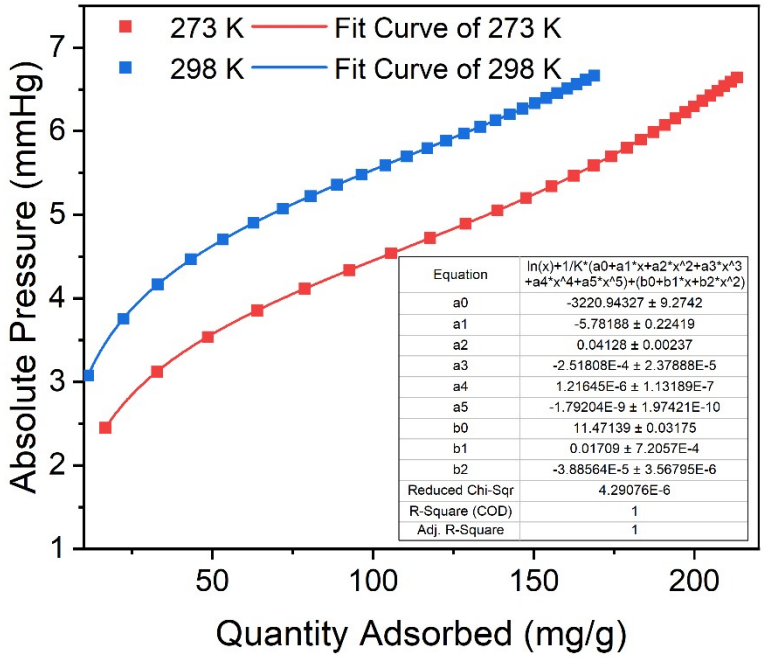

Fig. S10 Virial fitting of CO_2 for MIL-160.

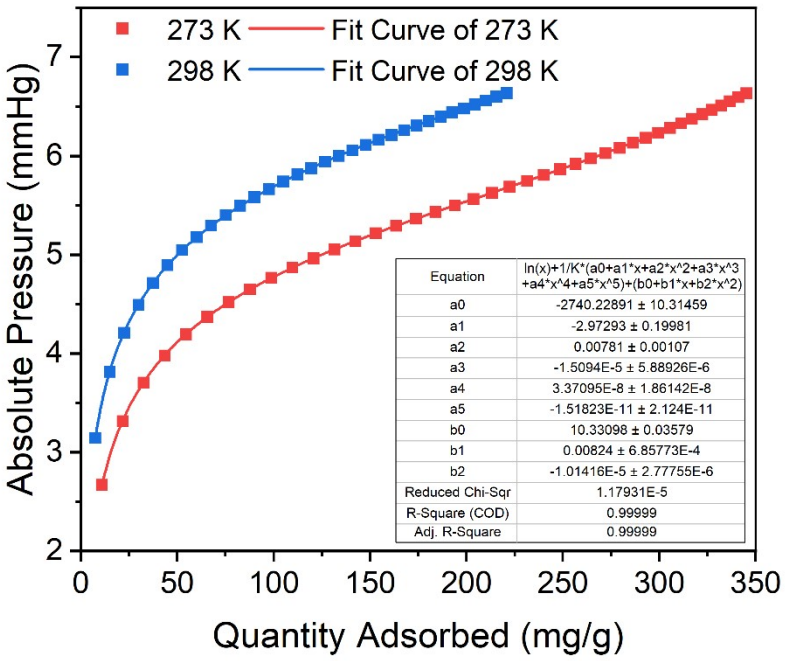

Equation	ln(x)+1/K*(a0+a1*x+a2*x^2+a3*x^3 +a4*x^4+a5*x^5)+(b0+b1*x+b2*x^2)
a0	-2740.22891 ± 10.31459
a1	-2.97293 ± 0.19981
a2	0.00781 ± 0.00107
a3	-1.5094E-5 ± 5.88926E-6
a4	3.37095E-8 ± 1.86142E-8
a5	-1.51823E-11 ± 2.124E-11
b0	10.33098 ± 0.03579
b1	0.00824 ± 6.85773E-4
b2	-1.01416E-5 ± 2.77755E-6
Reduced Chi-Sqr	1.17931E-5
R-Square (COD)	0.99999
Adj. R-Square	0.99999

Fig. S11 Virial fitting of CO_2 for MOF-303.

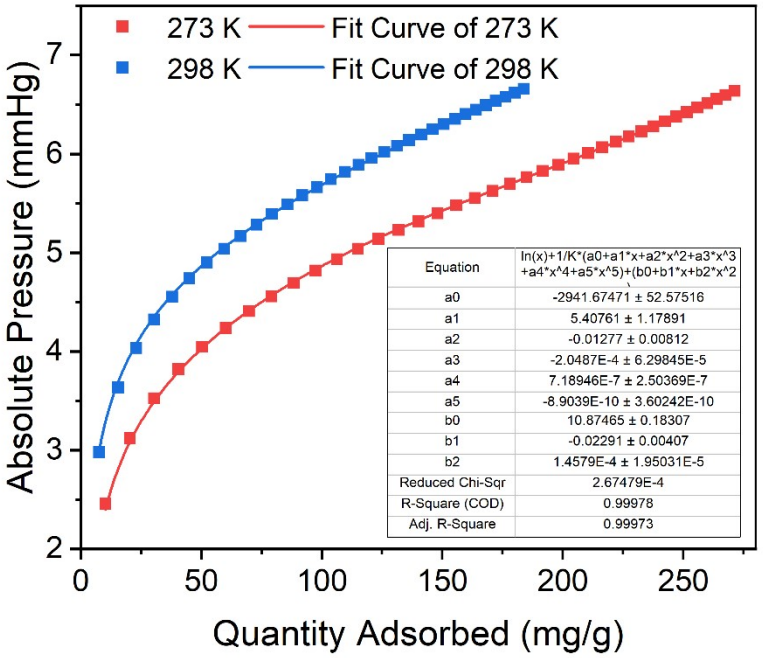

Equation	ln(x)+1/K*(a0+a1*x+a2*x^2+a3*x^3 +a4*x^4+a5*x^5)+(b0+b1*x+b2*x^2
a0	-2941.67471 ± 52.57516
a1	5.40761 ± 1.17891
a2	-0.01277 ± 0.00812
a3	-2.0487E-4 ± 6.29845E-5
a4	7.18946E-7 ± 2.50369E-7
a5	-8.9039E-10 ± 3.60242E-10
b0	10.87465 ± 0.18307
b1	-0.02291 ± 0.00407
b2	1.4579E-4 ± 1.95031E-5
Reduced Chi-Sqr	2.67479E-4
R-Square (COD)	0.99978
Adj. R-Square	0.99973

Fig. S12 Virial fitting of CO_2 for MOF-303/MIL-160.

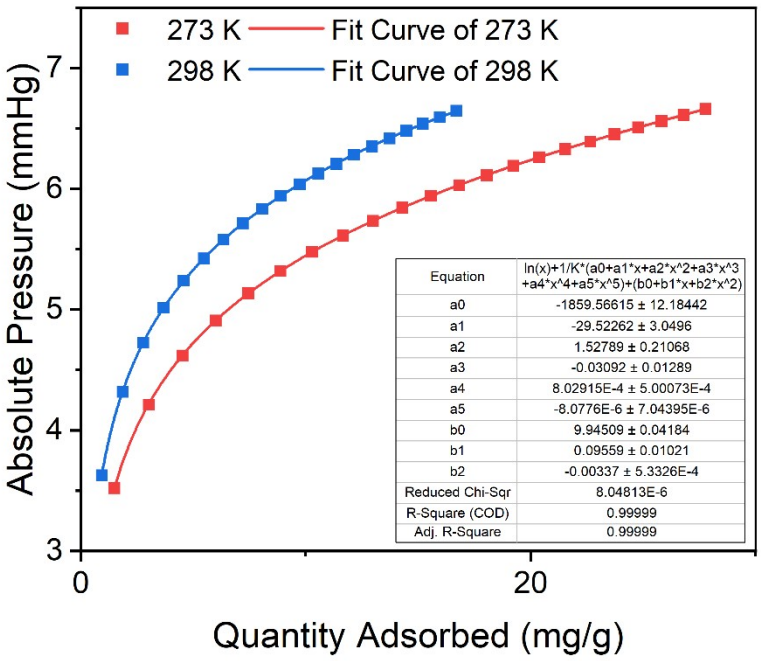

Fig. S13 Virial fitting of CH_4 for MIL-160.

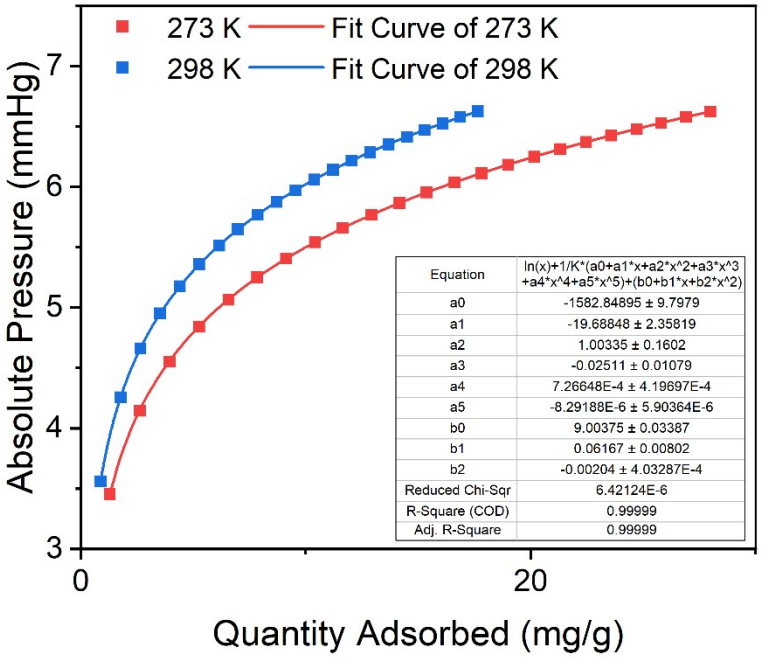

Fig. S14 Virial fitting of CH_4 for MOF-303.

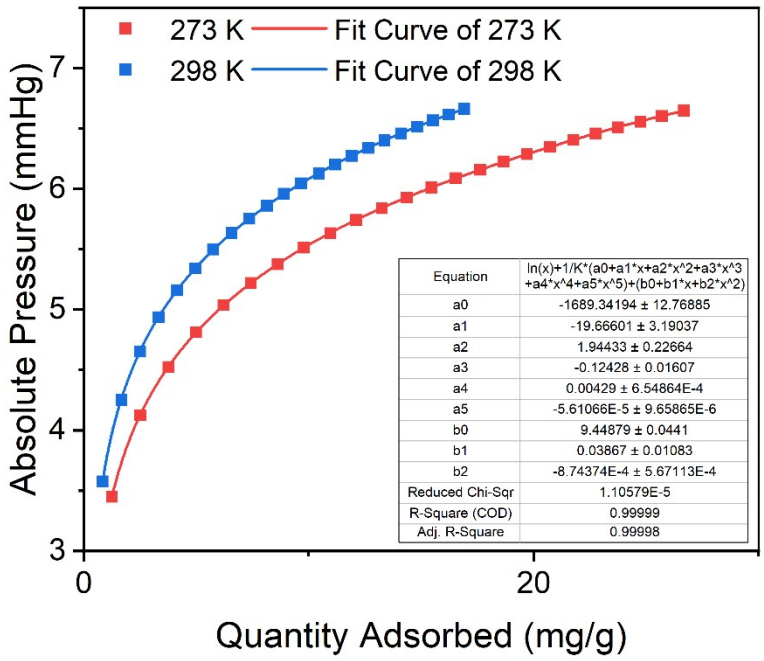

Equation	ln(x)+1/K*(a0+a1*x+a2*x^2+a3*x^3 +a4*x^4+a5*x^5)+(b0+b1*x+b2*x^2)
a0	-1689.34194 ± 12.76885
a1	-19.66601 ± 3.19037
a2	1.94433 ± 0.22664
a3	-0.12428 ± 0.01607
a4	0.00429 ± 6.54864E-4
a5	-5.61066E-5 ± 9.65865E-6
b0	9.44879 ± 0.0441
b1	0.03867 ± 0.01083
b2	-8.74374E-4 ± 5.67113E-4
Reduced Chi-Sqr	1.10579E-5
R-Square (COD)	0.99999
Adj. R-Square	0.99998

Fig. S15 Virial fitting of CH_4 for MOF-303/MIL-160.

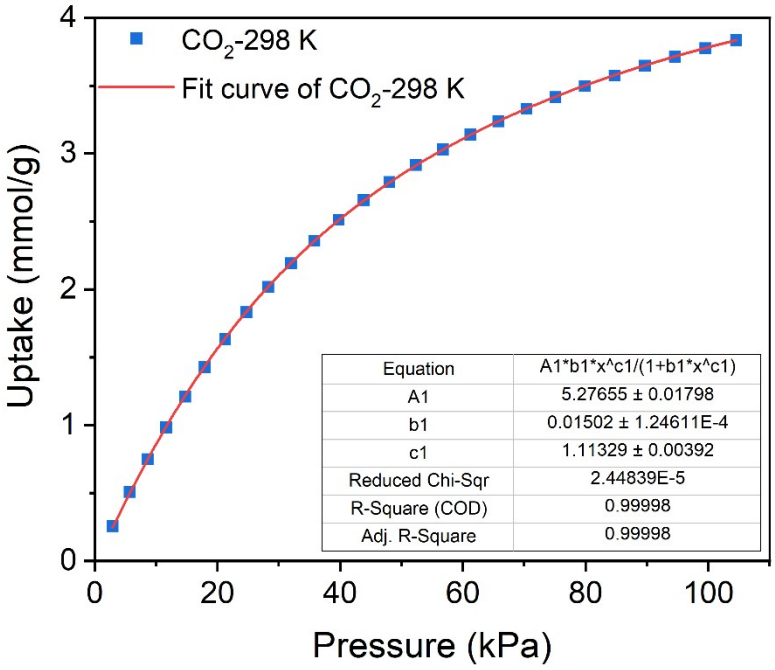

Equation	A1*b1*x^c1/(1+b1*x^c1)
A1	5.27655 ± 0.01798
b1	0.01502 ± 1.24611E-4
c1	1.11329 ± 0.00392
Reduced Chi-Sqr	2.44839E-5
R-Square (COD)	0.99998
Adj. R-Square	0.99998

Fig. S16 Langmuir-Freundlich fitting of CO_2 for MIL-160 at 298 K.

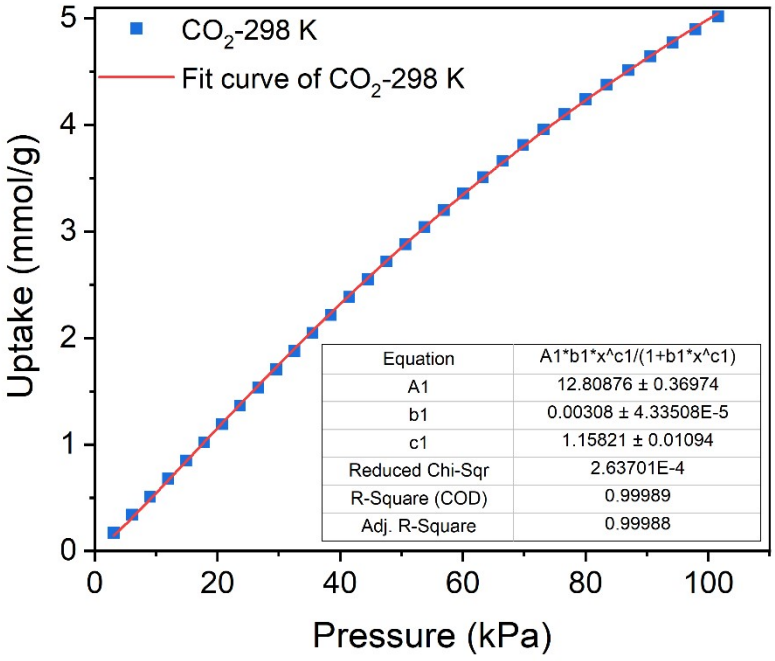

Fig. S17 Langmuir-Freundlich fitting of CO_2 for MOF-303 at 298 K.

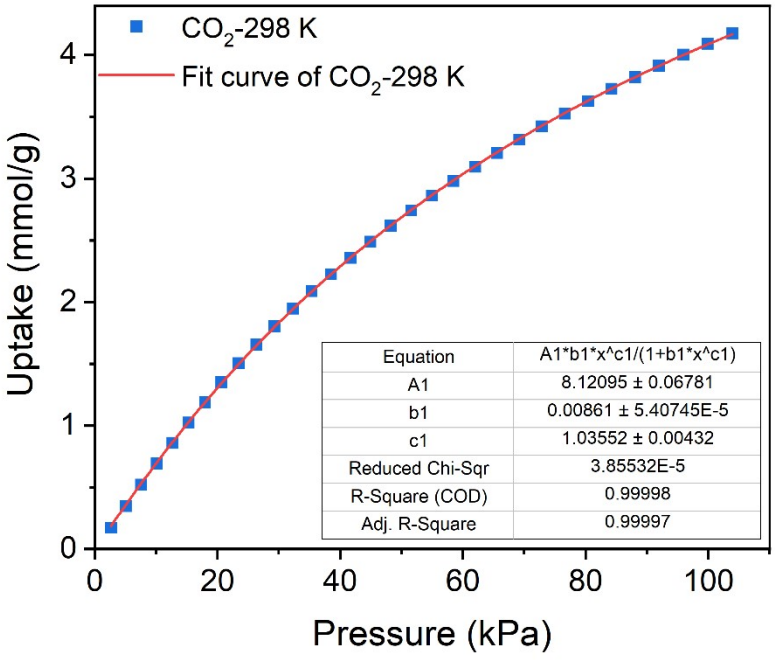

Fig. S18 Langmuir-Freundlich fitting of CO_2 for MOF-303/MIL-160 at 298 K.

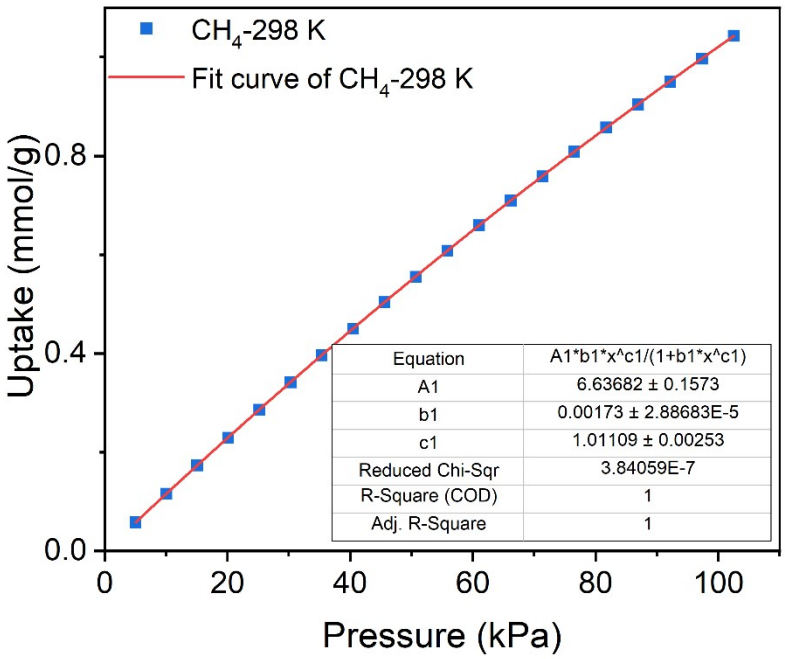

Fig. S19 Langmuir-Freundlich fitting of CH_4 for MIL-160 at 298 K.

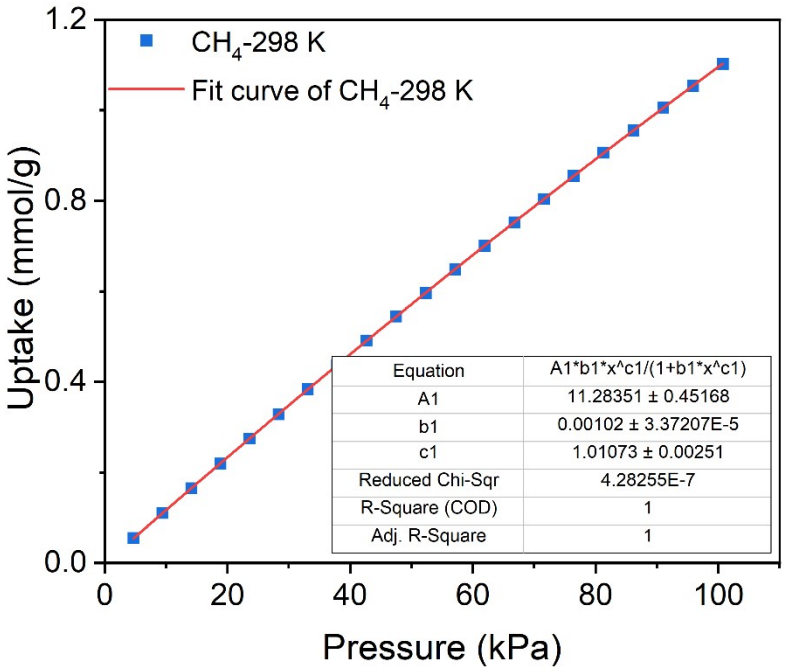

Fig. S20 Langmuir-Freundlich fitting of CH_4 for MOF-303 at 298 K.

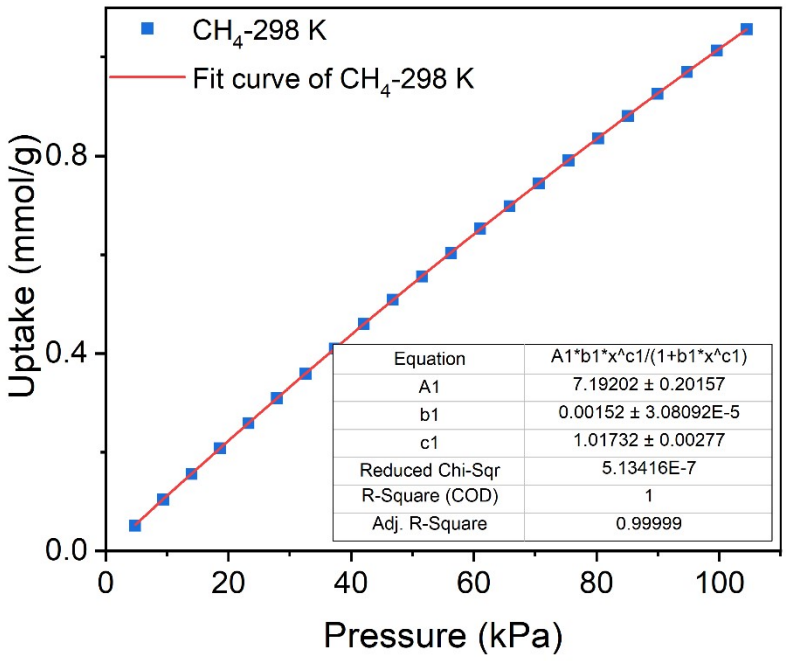

Fig. S21 Langmuir-Freundlich fitting of CH_4 for MOF-303/MIL-160 at 298 K.

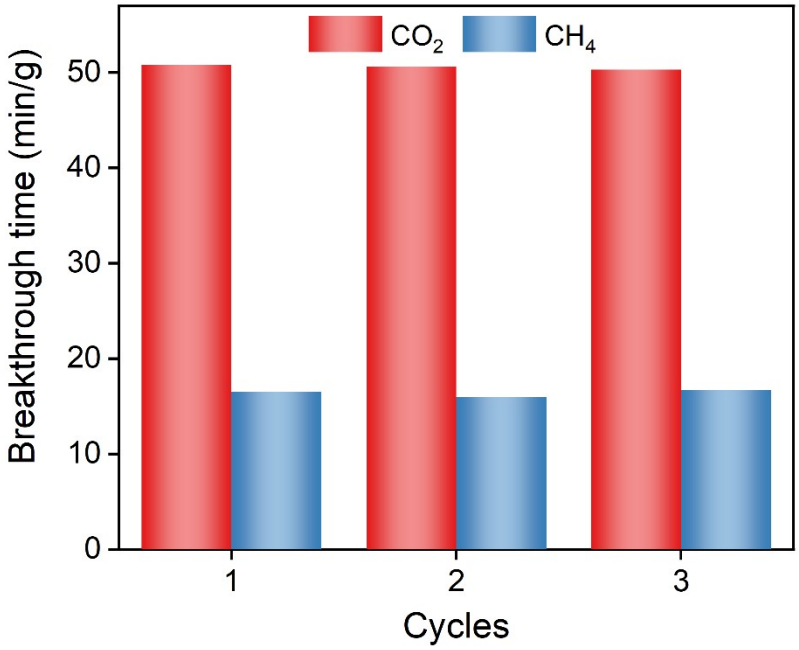

Fig. S22 Comparison of breakthrough time of CO_2 and CH_4 on MOF-303/MIL-160 in three consecutive cycles.

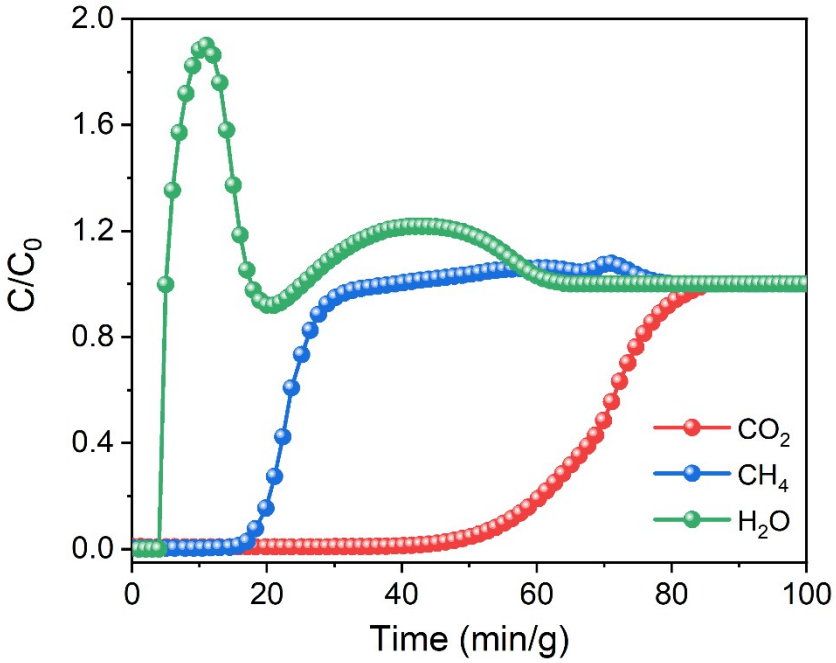

Fig. S23 Breakthrough curves of equimolar CO_2/CH_4 mixture (2 mL/min) on MOF-303/MIL-160 under humid condition (RH = 80%) at 298 K and 1 bar.

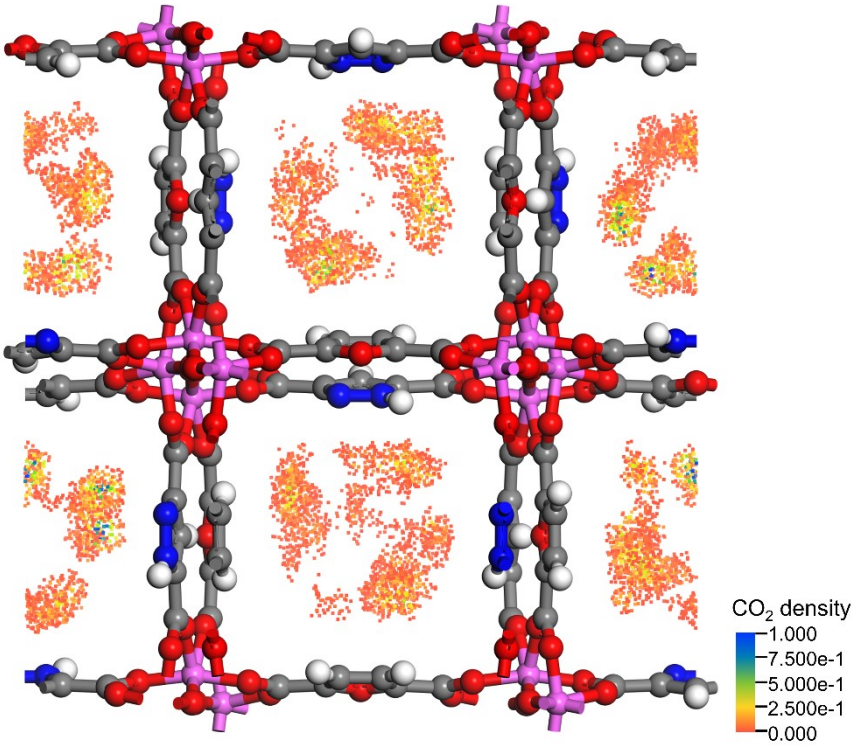

Fig. S24 Density distribution of CO_2 on MOF-303/MIL-160 at 100 kPa and 298 K.

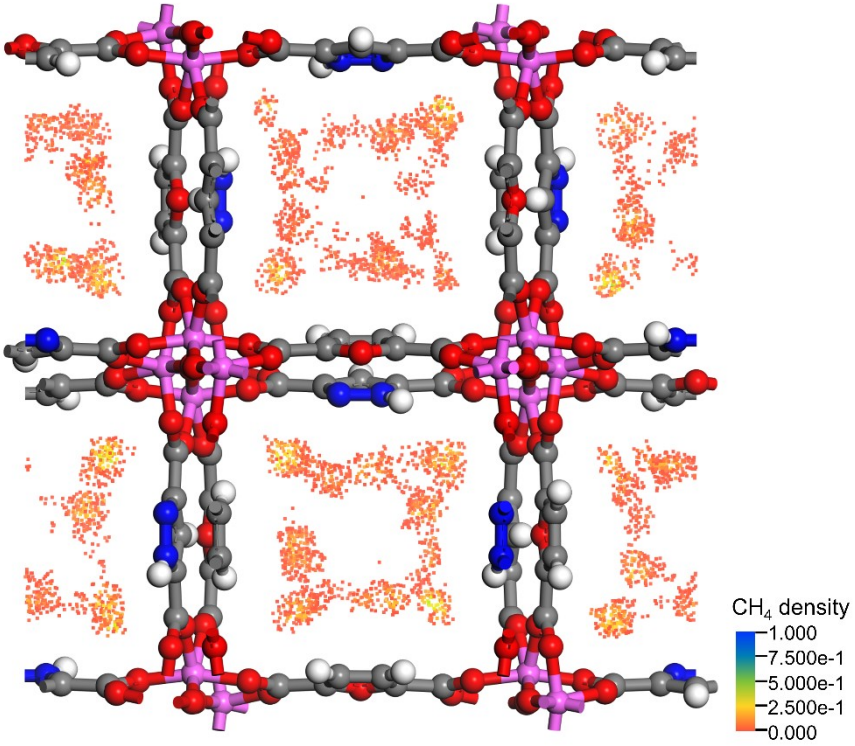

Fig. S25 Density distribution of CH_4 on MOF-303/MIL-160 at 100 kPa and 298 K.

Tables S1-S2

Table S1. Comparison of CO_2/CH_4 adsorption and separation performance in MOFs at 298 K.

Materials	CO_2 uptake (cm^3/g)	CH_4 uptake (cm^3/g)	CO_2 Q_{st} (kJ/mol)	CH_4 Q_{st} (kJ/mol)	IAST selectivity	Ref.
MOF-303/MIL-160	93.5	23.6	24.5	14.0	6.7	This work
MIP-202	12.44	0.90	30.7	–	72.9	[1]
NKU-521a	86	11	41	18	22	[2]
Cu-F-pymo	69.2	1.82	29.1	–	$>10^7$	[3]
FJU-44a	53.2	11.3	40.4	22.2	16	[4]
$ZnAtzCO_3$	62.8	14.7	32.6	22.4	151	[5]
NiNi-Pyz	92.5	32.3	30.0	23.7	7.2	[6]
SU-102	22.87	5.57	29.73	15.21	7.19	[7]
CPM-20(Co)	34	15	20.16	18.66	45	[8]
Zn-dmtrz-mip	65.4	19.7	26.5	–	17.8	[9]
MFM-126	103.7	20.0	30.7	17.3	11.7	[10]
MOF-801(Zr)	48.6	9.6	28.1	15.3	21.48	[11]
SNNU-325	41.5	16.4	19.1	18.4	4.0	[12]
Ni(dpip)	58.6	14.3	30.3	14.2	7.5	[13]
ZJNU-63	17.9	5.2	19.6	15.7	3.5	[14]
Cu-MTABA	33.6	11.9	38.5	16.1	9.94	[15]
CUMT-1	102.7	27.6	30.8	20.2	10.2	[16]

Table S2. Comparison of adsorption performance of MOF-303, MIL-160 and MOF-303/MIL-160.

Materials	MIL-160	MOF-303	MOF-303/MIL-160
BET surface area (m^2/g)	1110.4	1438.0	1348.3
CO_2 uptake at 273 K(cm^3/g)	108.5	175.6	138.0
CO_2 uptake at 298 K(cm^3/g)	85.9	112.4	93.5
CH_4 uptake at 273 K (cm^3/g)	38.8	39.1	37.3
CH_4 uptake at 298 K (cm^3/g)	23.3	24.6	23.6
CO_2 Q_{st} (kJ/mol)	26.7	22.7	24.5
CH_4 Q_{st} (kJ/mol)	15.4	13.1	14.0
IAST selectivity at 298 K	8.1	5.3	6.7

References

(1) Lv, D.; Chen, J.; Yang, K.; Wu, H.; Chen, Y.; Duan, C.; Wu, Y.; Xiao, J.; Xi, H.; Li, Z.; Xia, Q. Ultrahigh CO_2/CH_4 and CO_2/N_2 adsorption selectivities on a cost-effectively L-aspartic acid based metal-organic framework. *Chem. Eng. J.* **2019**, *375*, 122074. DOI: 10.1016/j.cej.2019.122074.

(2) Li, N.; Chang, Z.; Huang, H.; Feng, R.; He, W. W.; Zhong, M.; Madden, D. G.; Zaworotko, M. J.; Bu, X. H. Specific K^+ Binding Sites as CO_2 Traps in a Porous MOF for Enhanced CO_2 Selective Sorption. *Small* **2019**, *15* (22), 201900426. DOI: 10.1002/smll.201900426.

(3) Shi, Y.; Xie, Y.; Cui, H.; Alothman, Z. A.; Alduhaish, O.; Lin, R.-B.; Chen, B. An ultramicroporous metal–organic framework with dual functionalities for high sieving separation of CO_2 from CH_4 and N_2. *Chem. Eng. J.* **2022**, *446*, 137101. DOI: 10.1016/j.cej.2022.137101.

(4) Ye, Y.; Zhang, H.; Chen, L.; Chen, S.; Lin, Q.; Wei, F.; Zhang, Z.; Xiang, S. Metal–Organic Framework with Rich Accessible Nitrogen Sites for Highly Efficient CO_2 Capture and Separation. *Inorg. Chem.* **2019**, *58* (12), 7754–7759. DOI: 10.1021/acs.inorgchem.9b00182.

(5) Peng, J.; Fu, C.; Zhong, J.; Ye, B.; Xiao, J.; Duan, C.; Lv, D. Efficient Selective Capture of Carbon Dioxide from Nitrogen and Methane Using a Metal-Organic Framework-Based Nanotrap. *Molecules* **2023**, *28* (23), 7908. DOI: 10.3390/molecules28237908.

(6) Cai, Y.; Yong, J.; Chen, J.; Zhou, Y.; Gao, J. Hofmann-type metal-organic frameworks with dual open nickel centers for efficient capture of CO2 from CH_4 and N_2. *J. Solid State Chem.* **2022**, *315*, 123532. DOI: 10.1016/j.jssc.2022.123532.

(7) Li, C.-N.; Tao, Z.-P.; Liu, L.; Yuan, D.; Han, Z.-B. Cation exchange strategy of ellagic acid-based microporous metal-organic framework for efficient CO_2/N_2 and CO_2/CH_4 separation. *Chem. Eng. J.* **2024**, *502*, 157956. DOI: 10.1016/j.cej.2024.157956.

(8) Wu, B.-H.; Zhou, X.; Liu, L.; Han, Z.-B. A low cost and energy consumption Ultra-microporous CPM-20(Co) for CO_2/N_2 and CO_2/CH_4 separation. *J. Organomet. Chem.* **2024**, *1003*, 122922. DOI: 10.1016/j.jorganchem.2023.122922.

(9) Li, Y.-Z.; Wang, G.-D.; Lu, S.; Xu, F.; Zhang, H.; Sui, Y.; Hou, L. A moisture stable metal-organic framework for highly efficient CO_2/N_2, CO_2/CH_4 and CO_2/CO separation. *Chem. Eng. J.* **2024**, *484*, 149494. DOI: 10.1016/j.cej.2024.149494.

(10) Humby, J. D.; Benson, O.; Smith, G. L.; Argent, S. P.; da Silva, I.; Cheng, Y.; Rudić, S.; Manuel, P.; Frogley, M. D.; Cinque, G.; Saunders, L. K.; Vitórica-Yrezábal, I. J.; Whitehead, G. F. S.; Easun, T. L.; Lewis, W.; Blake, A. J.; Ramirez-Cuesta, A. J.; Yang, S.; Schröder, M. Host–guest selectivity in a series of isoreticular metal–organic frameworks: observation of acetylene-to-alkyne and carbon dioxide-to-amide interactions. *Chem. Sci.* **2019**, *10* (4), 1098–1106. DOI: 10.1039/c8sc03622e.

(11) Li, C.-N.; Wang, S.-M.; Tao, Z.-P.; Liu, L.; Xu, W.-G.; Gu, X.-J.; Han, Z.-B. Green Synthesis of MOF-801(Zr/Ce/Hf) for CO_2/N_2 and CO_2/CH_4 Separation. *Inorg. Chem.* **2023**, *62* (20), 7853–7860. DOI: 10.1021/acs.inorgchem.3c00560.

(12) Lei, J.; Zhang, P.; Xue, Y.-Y.; Xu, J.; Li, H.-P.; Lv, H.-J.; Wang, Y.; Li, S.-N.; Zhai, Q.-G. Design of ultra-stable Yttrium-organic framework adsorbents for efficient methane purification and storage. *Sep. Purif. Technol.* **2022**, *283*, 120211. DOI: 10.1016/j.seppur.2021.120211.

(13) Li, Y.-Z.; Wang, G.-D.; Ma, L.-N.; Hou, L.; Wang, Y.-Y.; Zhu, Z. Multiple Functions of Gas Separation and Vapor Adsorption in a New MOF with Open Tubular Channels. *ACS Appl. Mater. Interfaces* **2021**, *13* (3), 4102–4109. DOI: 10.1021/acsami.0c21554.

(14) Bai, D.; Wang, Y.; He, M.; Gao, X.; He, Y. Structural diversities and gas adsorption properties of a family of rod-packing lanthanide–organic frameworks based on cyclotriphosphazene-functionalized

hexacarboxylate derivatives. *Inorg. Chem. Front.* **2018**, *5* (9), 2227–2237. DOI: 10.1039/c8qi00575c.

(15) Das, P.; Mandal, S. K. Unprecedented High Temperature CO_2 Selectivity and Effective Chemical Fixation by a Copper-Based Undulated Metal–Organic Framework. *ACS Appl. Mater. Interfaces* **2020**, *12* (33), 37137–37146. DOI: 10.1021/acsami.0c09024.

(16) Lu, S.; Zhang, Y.-J.; Cheng, Y.-J.; Qin, Z.-H.; Wang, G.-D.; Bai, Y.; Lin, Y.; Wang, H.; Sui, Y.; Hou, L.; Li, Y.-Z. Capture of CO_2 from N_2 and CH_4 over a wide temperature range on a robust MOF with Brønsted acidic and Lewis basic dual functional sites. *J. Mater. Chem. A* **2025**, *13* (15), 10581–10589. DOI: 10.1039/d4ta08827a.